
Semi-Markov multistate modeling approaches for multicohort event history data

Xavier Piulachs*¹ | Klaus Langohr² | Mireia Besalú³ | Natalia Pallarès^{4,5} | Jordi Carratalà^{4,5,6} | Cristian Tebé^{4,5} | Guadalupe Gómez Melis²

¹Department of Statistics and Operations Research, Polytechnic University of Catalonia, Campus Terrassa, Spain

²Department of Statistics and Operations Research, Polytechnic University of Catalonia, Campus Barcelona, Spain

³Department of Genetics, Microbiology and Statistics, University of Barcelona, Barcelona, Spain

⁴Bellvitge Biomedical Research Institute, Bellvitge University Hospital, L'Hospitalet de Llobregat, Spain

⁵Department of Clinical Sciences, University of Barcelona, L'Hospitalet de Llobregat, Spain

⁶Department of Infectious Diseases, Bellvitge University Hospital, L'Hospitalet de Llobregat, Spain

Correspondence

*Xavier Piulachs, Department of Statistics and Operations Research, Polytechnic University of Catalonia, Campus Terrassa, Building TR5, C. Colom 11, 08222 Terrassa, Spain. Email: xavier.piulachs@upc.edu

Summary

Two Cox-based multistate modeling approaches are compared for modeling a complex multicohort event history process. The first approach incorporates cohort information as a fixed covariate, thereby providing a direct estimation of the cohort-specific effects. The second approach includes the cohort as stratum variable, thus providing an extra flexibility in estimating the transition probabilities. Additionally, both approaches may include possible interaction terms between the cohort and a given prognostic predictor. Furthermore, the Markov property conditional on observed prognostic covariates is assessed using a global score test. Whenever departures from the Markovian assumption are revealed for a given transition, the time of entry into the current state is incorporated as a fixed covariate, yielding a semi-Markov process. The two proposed methods are applied to a three-wave dataset of COVID-19-hospitalized adults in the southern Barcelona metropolitan area (Spain), and the corresponding performance is discussed. While both semi-Markovian approaches are shown to be useful, the preferred one will depend on the focus of the inference. To summarize, the cohort-covariate approach enables an insightful discussion on the behavior of the cohort effects, whereas the stratum-cohort approach provides flexibility to estimate transition-specific underlying risks according with the different cohorts.

KEYWORDS:

semi-Markov multistate model, cohort effect, heterogeneity, Markov test, COVID-19

1 | INTRODUCTION

Within the scope of biomedical studies, there is a rising interest in assessing the elapsed time from some predefined origin until the occurrence of a given terminal event among several mutually exclusive ones, competing with each other. As a natural extension of this competing risks setting, the analysis of intermediate clinical states over the follow-up period can also be addressed, thus giving a more comprehensive picture of a subject's trajectory through distinct states of a particular real-world complex process. This leads to modeling consecutively recorded event times, for which multistate models provide a natural framework (Andersen & Keiding, 2002; Houwelingen & Putter, 2008; Meira-Machado et al., 2009; Geskus 2015; Cook & Lawless, 2018). These models, typically specified in terms of the transition-specific hazards between subsequent states, allow us to enhance predictive performance regarding the probability of being in a particular state at a certain time.

This article describes two Cox-based multistate modeling approaches, termed M1 and M2, to analyze event history data that involves two commonly encountered technical difficulties. On the one hand, the typically adopted Markovian assumption for a given transition is not necessarily valid and needs to be checked. To this end, a global testing procedure for the Markov property is applied, so historical effects may be included in both the M1 and M2 approaches whenever a non-Markovian context is proven. On the other hand, the behavior of many infectious diseases may depend on temporal and population patterns. For instance, seasonal influenza may progressively affect different population cohorts over time (Darroch & McCloud, 1990), while Alzheimer’s disease affects distinct population groups differently (Birkenbihl et al., 2022). Moreover, disease outcomes may even vary based on the medical center at which the condition is treated (Freijser et al., 2023). In order for the unobserved cohort features influencing a given transition hazard to be properly incorporated, each of the two approaches introduces an alternative strategy. The M1 approach advocates including a cohort covariate, this becoming a particularly useful alternative when considering a reduced number of cohorts (Gelman & Hill, 2007). However, the cohort effect itself sometimes cannot be assigned a direct interpretation, with researchers being more interested in explaining how the impact of a baseline prognostic covariate changes with each cohort. In this case, an additional interaction term between the cohort and the covariate of interest should be added. Alternatively, assuming that the effect of observed prognostic covariates is of the highest interest, the M2 approach consists of stratifying a given transition hazard according to the disjoint cohorts. Here, a separate transition-specific baseline hazard function is estimated for each cohort, while preserving common coefficient estimates across cohorts for the prognostic covariates. As the price paid for stratification, the cohort effect is no longer included. On the other hand, estimates for the remaining covariates are more robust than in the M1 approach, though at the expense of some loss of efficiency (particularly when estimating transition probabilities between two states). Moreover, the interaction between the cohort and a particular covariate can still be assessed.

To illustrate the suggested modeling approaches, medical data on subjects hospitalized for severe coronavirus disease (COVID-19) is analyzed. Particularly, our applied research comes from the project entitled *Dynamic evaluation of COVID-19 clinical states and their prognostic factors to improve intra-hospital patient management* (Divine project), this data complying with the principles of the Declaration of Helsinki. The COVID-19 process comprises a finite number of intermediate, mutually-exclusive disease severity states, ranging from asymptomatic to critically ill subjects who require hospitalization (Huang et al., 2020; Chan et al., 2020). Among the latter, the course of COVID-19 can induce severe pneumonia, which can lead to the need for ventilatory support or even to death. Additionally, this pathological process involved a significant heterogeneity in the degree of severity between subjects, as the waves of the pandemic ebbed and flowed over time (Carbonell et al., 2021; Buttenschon et al., 2022). As part of the Divine project, it is of major interest to elucidate subject-specific changes in mortality trends when analyzing data from the first three COVID-19 waves in Spain. To avoid selection bias, only subjects who were infected before hospital entry were selected, as well as subjects without a predetermined ceiling of care (i.e., those deemed suitable to receive advanced care). Further, virtually none of the subjects under study had received a COVID-19 vaccine prior to hospital admission. Although a considerable proportion of the world’s population is now vaccinated, an added value of our observational data is that it provides a comprehensive multistate modeling framework to understand and compare the information from the three distinct COVID-19 waves that occurred during the most complicated time period of the disease.

Our two Cox-based multistate modeling approaches are proposed to (i) assess the Markov hypothesis for all the relevant transitions in a multistate process, and (ii) quantify how cohort membership interacts with some baseline prognostic covariate when modeling a given transition hazard to the next state. Basically, both approaches account for past-history influence whenever the Markovian condition does not hold, while respectively applying the above mentioned strategies to incorporate the influence of the cohort. Each strategy has its strengths and weaknesses, and determines the type of information that may be derived from the approach. The remainder of the paper proceeds as follows. Section 2 introduces the motivating study of the methods presented, consisting of a large longitudinal dataset of adults with confirmed COVID-19 infections who were hospitalized during one of the first three coronavirus waves in the southern Barcelona metropolitan area. Section 3 describes the M1 and M2 approaches for modeling a given transition hazard. Section 4 illustrates the application of our two approaches to the motivating event history data. Lastly, Section 5 discusses the main results and suggests some possible directions for future research.

2 | THREE-WAVE COVID-19 DATA IN THE SOUTHERN BARCELONA URBAN AREA

The motivating three-wave data, which will be referred to as the *div3W* data, covers a part of the database from the Divine project and comprises $n = 3290$ COVID-19-hospitalized adults without a ceiling of care. They were admitted during the first three COVID-19 waves occurring in Spain, spanning from March 2020 to February 2021, to five collaborating medical centers located

in the southern Barcelona metropolitan area. There were 2074 subjects recruited during the first wave, March–April 2020, 611 subjects during the second wave, October–November 2020, and 605 subjects during the third wave, January–February 2021. None of the individuals were lost to follow-up after hospital admission, so they were all monitored until either hospital discharge or death. Figure 1 shows the unidirectional multistate scheme used for modeling subject flow in the COVID-19 hospitalization process across the three waves, together with the number of individuals in each wave passing from one state to other. Upon being admitted to hospital (state 0), subjects are immediately assigned to one of the two possible initial states according to the severity of disease: no severe pneumonia, NSP (state 1) and severe pneumonia, SP (state 2); thus, all hospitalized subjects are in one of these two states at $t = 0$. Subjects can then pass through three intermediate disease states: recovery (state 3), noninvasive mechanical ventilation, NIMV (state 4), and invasive mechanical ventilation, IMV (state 5). Finally, subjects can move to only one of two final states: discharge (state 6) or death (state 7). The following are particularly important features of this scheme. First, our data does not report the exit times from the SP, NIMV and IMV states to the recovery state. We therefore do not know the exact time point at which the subjects returned to the hospital ward before being subsequently discharged. To remedy this, these individuals are assigned a fixed 2-day stay in recovery, this period being the minimum transition time required from a medical standpoint. Second, a very small number of subjects are reported in at least one of the waves for the SP → death, recovery → death, and NIMV → death transitions; indeed, the small quantities observed in the first wave are even lower in the subsequent ones. These transitions correspond to individuals who died prematurely either in the early and noncritical states, or without undergoing IMV, so in a way they experienced an unnatural in-hospital trajectory. Even though the number of these subjects is not particularly large across the different waves, it became lower as the pandemic unfolded and disease knowledge increased. Third, the subject's entry into the intensive care unit is not considered here as a state itself. The reason is that each medical center established its own criterion for ICU assignment according to the bed occupancy level, so a hypothetical ICU state would involve as many criteria as hospitals considered, possibly yielding misleading conclusions.

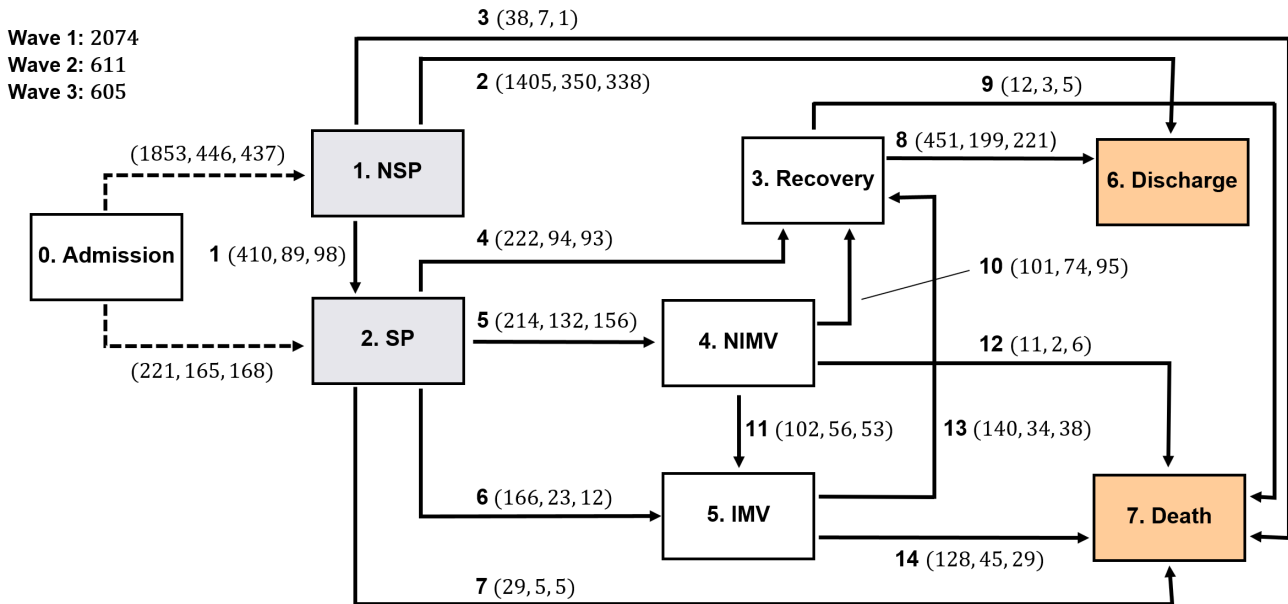


Figure 1 Multistate scheme adopted for modeling the clinical trajectory of the COVID-19-hospitalized subjects from the div3W data. The in-hospital course of COVID-19 disease is divided for each wave into seven states after hospital admission: 1) no severe pneumonia (NSP), 2) severe pneumonia (SP), 3) recovery, 4) noninvasive mechanical ventilation (NIMV), 5) invasive mechanical ventilation (IMV), 6) discharge, and 7) death. The model envisages 14 possible transitions (solid arrows) between a pair of states, while it implicitly accounts for two instantaneous transitions (dashed arrows) from admission to either NSP or SP. Within each wave, the number of subjects observed per transition is indicated.

The div3W data also provides a number of demographic and medical characteristics recorded upon hospital admission. Table 1 summarizes the characteristics of the baseline prognostic covariates selected in our study following expert consultation, all

assumed to be independently associated with the in-hospital mortality risk during each wave. We refer to Pallarès et al. (2023) for further details regarding these covariates, which are in line with the most frequently used information in the COVID-19 literature (Wendel-Garcia et al. 2021, Berenguer et al. 2021). Together with sex and age variables, the value of the safi ratio (Catoire et al., 2021) is used as illness severity scores. The safi value describes the relationship between the peripheral arterial oxygen saturation, typically ranging from 95% to 100%, and the fractional inspired oxygen concentration, with a value of 0.21 at room air. A better health condition is then related to higher safi values, with the interval [300, 476.2] covering most of the subjects considered.

Across the three waves, more than half of the subjects are men, and a slight increase in age is observed as the pandemic progressed. It is also found that the proportion of subjects affected by SP is drastically higher in the later waves, and there is also a sharp increase in the proportion of subjects moving from SP to either NIMV or IMV; the latter account for 380 subjects in the first wave (18.3%), 155 subjects in the second wave (25.4%), and 168 subjects in the third wave (27.8%). These observed trends in age and disease severity, that might seem to behave in a counterintuitive way, can be explained by a relaxation in the ceiling-of-care criteria as the pandemic evolved, leading to a progressive increase in more critically ill subjects being admitted to hospital. Thus, as the strong restrictions during the first wave gradually disappeared, the subsequent waves saw a higher admission rate for elderly subjects to the healthcare system; these subjects are the most seriously affected by the disease and often have multiple comorbidities. By contrast, a larger proportion of subjects died in the hospital during the first and second waves than during the third one.

Table 1 Baseline characteristics of COVID-19-hospitalized subjects from the div3W data throughout the first, second, and third pandemic waves. Categorical covariates are expressed as counts and percentages (%), whereas continuous covariates are expressed as medians and interquartile ranges (IQR). The selected baseline covariates are sex (female indicator), age (years), and the safi value (units).

Characteristics	Wave 1 ($n = 2074$)	Wave 2 ($n = 611$)	Wave 3 ($n = 605$)
Baseline covariates			
Sex (female)	854 (41.2%)	222 (36.3%)	248 (40.1%)
Age (years)	59 (49 – 69)	62 (53 – 71)	63 (52 – 72)
Safi value (units)	447.6 (395.2 – 461.9)	442.9 (346.4 – 457.1)	438.1 (342.9 – 457.1)
Illness time course			
SP	631 (30.4%)	254 (41.6%)	264 (43.8%)
NIMV	214 (10.3%)	132 (21.6%)	156 (25.8%)
IMV	268 (12.9%)	79 (12.9%)	65 (10.7%)
In-hospital mortality	218 (10.5%)	62 (10.1%)	46 (7.6%)

3 | SEMI-MARKOV MULTISTATE MODELING FOR MULTIPLE COHORTS

3.1 | General framework

Consider a finite set of mutually-exclusive states $\mathcal{R} = \{1, \dots, R\}$, $R \in \mathbb{N}$, and let $\{X_i(t), t \geq 0\}$, $i = 1, \dots, n$, denote the stochastic process that indicates the state occupied by the i th subject at a particular time point t within a bounded time interval of interest $[0, \tau]$. The random process $X_i(t)$ is allowed to have independent, right-continuous sample trajectories on $[0, \infty)$. Consider also the σ -algebra that informs about the subject's complete disease state history until t , say $\mathcal{H}_i(t) = \{X_i(u), 0 \leq u \leq t\}$. The multistate structure can be completely characterized by the transition hazard between subsequent states $\{\ell, m\} \in \mathcal{R}, \ell \neq m$, defined as the i th subject's instantaneous cause-specific hazard per time unit of going from the state ℓ to the state m . Formally,

$$h_i^{\ell m}\{t \mid \mathbf{z}_i, \mathcal{H}_i(t)\} = \lim_{dt \rightarrow 0} \frac{\Pr \{X_i(t + dt) = m \mid X_i(t) = \ell; \mathbf{z}_i, \mathcal{H}_i(t)\}}{dt}, \quad t > 0, \quad (1)$$

so that the above hazard-based measure is conditioned on: the current time t , a p -dimensional vector of baseline prognostic covariates (possibly different for each transition), $\mathbf{z}_i = (z_{1i}, \dots, z_{pi})^\top$, and the historical information up to immediately before

time t , $\mathcal{H}_i(t)$. As the other key element within the multistate modeling framework, one can define the transition probability between any pair of states, even if they are not subsequent. This is postulated as the i th subject's probability of being in state m at time t conditional on occupying the state ℓ at time s , with $s < t$, along with the subject's characteristics \mathbf{z}_i and $\mathcal{H}_i(s)$:

$$P_i^{\ell m}(s, t) = \Pr\{X_i(t) = m \mid X_i(s) = \ell, \mathbf{z}_i, \mathcal{H}_i(s)\}, \quad s < t. \quad (2)$$

For estimation purposes, the underlying multistate process is typically assumed to be Markovian conditional on transition-specific covariates, so the future and the past history are independent given the present. In practice, the effect of $\mathcal{H}_i(t)$ disappears, which greatly simplifies the parameter estimation procedure. Under a nonparametric Markovian framework, the product-limit relation given by the Aalen-Johansen (AJ) estimator (Aalen & Johansen, 1978) provides an easy-to-compute way to translate the $\ell \rightarrow m$ transition intensities at any t into consistent estimates for the transition probabilities. If using a Cox semiparametric model (Cox, 1972) to introduce prognostic covariates \mathbf{z}_i in transition hazards, the AJ estimator can also be applied to estimate the corresponding transition probabilities (Andersen et al., 1991). In contrast, when departing from the Markov condition, explicit formulas for the transition probabilities may be challenging to derive (Meira-Machado et al., 2006; Andersen & Perme, 2008; Titman, 2015). The Markov assumption is, nevertheless, a quite restrictive hypothesis whose appropriateness needs to be properly verified to prevent misleading results.

The whole multistate process can be modeled by separately fitting a semiparametric Cox model for each transition hazard, which allows researchers to incorporate the effect of prognostic covariates. Under this framework, a subject's past history can be easily considered in the $\ell \rightarrow m$ transition by including some functional form $f(\cdot)$ of the time $t_{\ell i}$ at which the current state ℓ is reached. For conciseness, $f(\cdot)$ is assumed to be the identity, although nothing prevents us from employing a more suitable functional form, such as high-order polynomials or splines. The subject's instantaneous hazard is written as

$$h_i^{\ell m}(t \mid \mathbf{z}_i, t_{\ell i}) = h_0^{\ell m}(t) \exp\{(\boldsymbol{\beta}^{\ell m})^\top \mathbf{z}_i + \gamma^{\ell m} t_{\ell i}\}, \quad (3)$$

where $h_0^{\ell m}(t)$ is an arbitrary nonnegative transition-specific baseline hazard function permitted to vary over time, $\boldsymbol{\beta}^{\ell m} = (\beta_{z_1}^{\ell m}, \dots, \beta_{z_p}^{\ell m})^\top$ is a vector of p unknown regression coefficients corresponding to \mathbf{z}_i , and $\gamma^{\ell m}$ is an unknown coefficient related to $t_{\ell i}$; whenever the Markovian rule holds, $\gamma^{\ell m} = 0$. We therefore have a semi-Markov multistate model in which the subject's historical effects are accounted for via the covariate describing the time of entry into the current state $t_{\ell i}$. It is worth mentioning that this latter time does not entail a new time scale, but simply incorporates a time-of-entry covariate whose value is automatically established for those subjects who reach the ℓ state. As another point, the semiparametric Cox model assumes both the proportional hazards hypothesis (i.e., constant effect of a given covariate on the hazard over the follow-up period) and a log-linear association between the transition hazard and covariate. Consequently, both hypotheses should be checked.

Estimates for $\boldsymbol{\beta}^{\ell m}$ and $\gamma^{\ell m}$ are found by maximizing the Cox partial log-likelihood function for the transition at hand, whereas the Breslow estimator (Breslow, 1972) provides a nonparametric estimate for the corresponding cumulative baseline hazard function. Here, the `mstate` package (Putter et al., 2007) from the R environment is used to perform the multistate model fitting, with each transition-specific Cox model being fitted independently; this entails a more efficient method than maximizing the full joint likelihood function over all transitions (Ieva et al., 2017). Further details regarding parameter estimation can be consulted, for example, in de Wreede et al. (2010).

3.2 | Testing the Markov hypothesis

We describe two existing methods for testing the Markov assumption when modeling transition intensities under a semi-Markov Cox-based framework. On the one hand, a general procedure is applied for revealing discrepancies with respect to the Markov property in any given Cox-like transition hazard. This procedure involves a global test score, computed in a summarized manner from a family of local log-rank tests whose p -values are obtained via subsampling techniques. On the other hand, as a more particular alternative, one may include a covariate which collects certain aspect of the past history. This is a useful way to proceed when such an aspect may be held liable for departures from the Markovian behavior.

3.2.1 | Likelihood ratio test to detect any relevant aspect from past history

Consider an $\ell \rightarrow m$ transition hazard that has been estimated by means of a Cox regression model. To test the Markov assumption, the simplest procedure consists of capturing the subject's past history by including the corresponding time of entry $t_{\ell i}$ into the current state ℓ . This provides a rapid and easy manner for checking the Markov hypothesis through a likelihood ratio test of

$\gamma^{\ell m} = 0$, at a given significance level α . Of note, an alternative interpretation of such an entry time could be derived by assuming the transformation $t_{\ell i} = t - (t - t_{\ell i})$. This yields (3) to be rewritten as

$$h_i^{\ell m}(t \mid \mathbf{z}_i, t_{\ell i}) = h_0^{\ell m}(t) \exp(\gamma^{\ell m} t) \exp\{(\boldsymbol{\beta}^{\ell m})^\top \mathbf{z}_i - \gamma_{\mathcal{H}}^{\ell m}(t - t_{\ell i})\},$$

providing a direct association between the hazard and both the chronological time t , collected via the baseline hazard function, and the sojourn time in the state ℓ , i.e., $t - t_{\ell}$. The latter, however, has a regression coefficient of opposite sign to t_{ℓ} , so the association with the transition hazard should now be interpreted in the reverse sense. Throughout the article, the results will be presented relating to the effect of t_{ℓ} , unless otherwise specified.

As in the Markov environment, an advantageous characteristic of the Cox semi-Markov multistate model relies on its ease of implementation with standard software. Obviously, alternative choices for tackling historical follow-up could be considered (e.g., the number of states that a subject has gone through prior to entering into the state ℓ). The choice of one or the other depends on the degree of understanding about the process.

3.2.2 | Global score test for the Markov assumption

Taking the so-called landmark techniques (de Uña-Álvarez & Meira-Machado, 2015; Putter & Spitoni, 2018) as a starting point, Titman and Putter (2022) have recently proposed a Cox-based global test for assessing the Markov assumption conditional on transition-specific covariates. Let j be a qualifying state for the $\ell \rightarrow m$ transition, and $Y_i(t)$ be the subject's at-risk indicator within the multistate process. For a given landmark time s , consider the subsamples $\mathcal{S} = \{i : X_i(s) = j, Y_i(s) = 1\}$ and $\mathcal{S}^c = \{i : X_i(s) \neq j, Y_i(s) = 1\}$. We can test the Markov property by focusing on the i th subject's membership in \mathcal{S} . Under Markovian conditions, transition probabilities are straightforwardly obtained from transition intensities, so differences between \mathcal{S} and \mathcal{S}^c can be assessed by merely testing

$$H_0 : h_i^{\ell m}\{t \mid \mathbf{z}_i, X_i(s) = j\} = h_i^{\ell m}\{t \mid \mathbf{z}_i, X_i(s) \neq j\} \text{ for } t \geq s, \text{ against any other alternative.} \quad (4)$$

Testing this hypothesis is carried out via a global score test constructed for Cox-based transition intensities. Specifically, let $\delta_i^{(j)}(s) = I\{X_i(s) = j\}$ be the membership indicator for the j state. Let also $Y_{i\ell}(t) = I\{X_i(t^-) = \ell\}Y_i(t)$ be the at-risk indicator for the $\ell \rightarrow m$ transition, and $N_i^{\ell m}(t)$ the counting process reporting the number of stochastic movements between ℓ and m up to time t . Under a Cox-Markov multistate model, H_0 can be tested via the log-rank statistic

$$U^{\ell m(j)}(s, \boldsymbol{\beta}^{\ell m}) = \sum_{i=1}^n \int_s^\tau \left\{ \delta_i^{(j)}(s) - \frac{\sum_{r=1}^n \delta_r^{(j)}(s) Y_{r\ell}(t) \exp\{(\boldsymbol{\beta}^{\ell m})^\top \mathbf{z}_r\}}{\sum_{r=1}^n Y_{r\ell}(t) \exp\{(\boldsymbol{\beta}^{\ell m})^\top \mathbf{z}_r\}} \right\} dN_i^{\ell m}(t), \quad t > s, \quad (5)$$

which acts as a score statistic for $\delta_i^{(j)}(s)$ when replacing $\boldsymbol{\beta}^{\ell m}$ with its maximum partial likelihood estimate, $\hat{\boldsymbol{\beta}}^{\ell m}$. The first term from the difference in (5) checks whether a subject is actually in the j state at time s or not, whereas the second term is the probability that a subject transitioning at time t was previously in j at time s , conditional on the set of subjects in ℓ at time t . It is essentially a testing procedure involving the comparison of the future rate for the possible $\ell \rightarrow m$ transitions across the different groups defined by the j state occupied at time s . Thus, $U^{\ell m(j)}(s, \hat{\boldsymbol{\beta}}^{\ell m})$ will differ from zero when the probability to reach the ℓ state differs provided that $X_i(s) \neq j$.

Because time s is allowed to vary over a period $[t_0, t_{\max}] \subset [0, \tau]$, a sequence of tests like (4) can be longitudinally conducted over a grid $\{s_1, \dots, s_L\} \in [t_0, t_{\max}]$, adequately chosen to avoid intervals with a small number of subjects. A log-rank test statistic vector $\{U^{\ell m(j)}(s_1, \hat{\boldsymbol{\beta}}^{\ell m}), \dots, U^{\ell m(j)}(s_L, \hat{\boldsymbol{\beta}}^{\ell m})\}$ is then obtained, which is proven to be asymptotically independent and zero-mean normal under H_0 . Thus, the standardized process

$$\bar{U}^{\ell m(j)}(s, \hat{\boldsymbol{\beta}}^{\ell m}) = U^{\ell m(j)}(s, \hat{\boldsymbol{\beta}}^{\ell m}) / [\text{Var}^{\ell m(j)}(s, \hat{\boldsymbol{\beta}}^{\ell m})]^{1/2}, \quad s \in [t_0, t_{\max}],$$

converges to a standard normal distribution, approximated by repeatedly generating a large number of resamples (a minimum of 1000 is recommended to perform the test) via wild bootstrapping methods (Mammen, 1993). Three summary test statistics are compared according to different assumptions regarding how the past-history effect is considered when computing (5). The absolute mean, $\int_{t_0}^{t_{\max}} |\bar{U}^{\ell m(j)}(s, \hat{\boldsymbol{\beta}}^{\ell m})| ds$, assumes identical importance for all landmark times. The weighted absolute mean, $\int_{t_0}^{t_{\max}} |w(s) \bar{U}^{\ell m(j)}(s, \hat{\boldsymbol{\beta}}^{\ell m})| ds$ involves weights $w(s)$ chosen to overweight the influence of times in which it is more likely to detect Markovian departures. The absolute maximum $\sup_{s \in [t_0, t_{\max}]} |\bar{U}^{\ell m(j)}(s, \hat{\boldsymbol{\beta}}^{\ell m})|$ only accounts for the time with the most important deviation from the Markov property. By accurately combining the p -values derived from the sequence of standardized statistics, a global p -value for testing the Markov property in the selected transition can then be returned; the lower the p -value, the stronger the suggestion that the Markovian assumption is not tenable. Further, when handling multiple interconnected states, a given

landmark s can be associated with two or more qualifying states $\{j_1, j_2, \dots\}$ from which the $\ell \rightarrow m$ transition is reachable, yielding $\{\bar{U}^{\ell m(j_1)}(s, \hat{\beta}^{\ell m}), \bar{U}^{\ell m(j_2)}(s, \hat{\beta}^{\ell m}), \dots\}$. Here, the Markov assumption can be globally evaluated by means of an overall chi-squared test statistic $T^{\ell m(j)}(s, \hat{\beta}^{\ell m})$ obtained from $\sum \{\bar{U}^{\ell m(j)}(s, \hat{\beta}^{\ell m})\}^2$, so that an overall p -value can be given.

Complete details on the above testing procedure, as well as on how to choose summaries and weights, are given in the aforementioned Titman and Putter's article. The test is implemented in the R package `mstate` through the built-in function termed `MarkovTest`.

3.3 | Formulation of the two Cox-based multistate modeling approaches

From the Cox-based transition hazard postulated in (3), the multistate modeling approaches M1 and M2 are considered for analyzing event history data from disjoint cohorts. The motivation behind both approaches is to account for possible inter-cohort heterogeneity in the target population, which ultimately may allow us to infer cohort-specific medical conclusions. Let us consider a heterogeneous target population that can be split into $G > 1$ cohorts of subjects. The i th subject's cohort membership, say $g = 1, \dots, G$, is accounted for by $G - 1$ binary indicators, namely $\{c_{gi}, g \geq 2\}$, where $c_{gi} = 1$ if the subject is actually in cohort $g \in \{2, \dots, G\}$, or $c_{gi} = 0$ otherwise. For the particular case $c_{2i} = \dots = c_{Gi} = 0$, the subject is part of the first cohort, $g = 1$. The way in which the information about cohorts is accounted for yields the approaches that are detailed next.

3.3.1 | M1 Approach: Inclusion of a cohort effect and its interaction with a covariate

The M1 approach accounts for the multicohort nature of the data by simultaneously adding two terms in a Cox transition hazard. To begin with, we incorporate a collection of $G - 1$ cohort binary regressors as fixed effects, along with their corresponding regression parameters. However, rather than considering the cohort effect in isolation, one may be more interested in assessing how the strength of association between a generic transition hazard and a given prognostic covariate at baseline is modulated by the effect of a specific cohort. Hence, attention can be restricted to exploring whether the relationship between the $\ell \rightarrow m$ transition-specific hazard and a particular time-fixed predictor z_q from vector \mathbf{z} , with $q \in \{1, \dots, p\}$, may vary across the distinct cohorts. When assessing this potential dependency, the fixed-effects M1 approach advocates for also including an interaction term between the cohort g and the baseline prognostic covariate z_q . This yields the following Cox proportional hazards regression model whenever a given subject i is in the cohort g :

$$h_i^{\ell m}(t \mid \mathbf{z}_i, t_{\ell i}, c_{gi} = 1) = h_0^{\ell m}(t) \exp \left\{ (\boldsymbol{\beta}^{\ell m})^\top \mathbf{z}_i + \gamma^{\ell m} t_{\ell i} + \eta_g^{\ell m} + \eta_{g \times z_q}^{\ell m} z_{qi} \right\}. \quad (6)$$

To quantify the effect of parameters from the above Cox-based regression, the transition-specific hazard ratio is typically used. This quantifies the change in $h_i^{\ell m}(\cdot)$ for an increase of Δ units in the q th covariate, while conditioning on the cohort. Assuming z_q as continuous in the remainder of the article, the corresponding conditional hazard ratio is defined at any time t by

$$\text{HR}_{z_q|g}^{\ell m} = \exp \left\{ (\beta_{z_q}^{\ell m} + \eta_{g \times z_q}^{\ell m}) \Delta \right\}. \quad (7)$$

A question of interest lies then in testing whether, conditional on the cohort g , the hazard ratio associated to a Δ -unit increase in z_q changes significantly. We then perform the test

$$H_0: \eta_{2 \times z_q}^{\ell m} = \dots = \eta_{G \times z_q}^{\ell m} = 0 \text{ against } H_A: \exists g \in \{2, \dots, G\} \text{ such that } \eta_{g \times z_q}^{\ell m} \neq 0, \quad (8)$$

which can be conducted using a likelihood ratio test.

On the other hand, we can compare the transition hazard of a subject from the cohort $g \in \{2, \dots, G\}$ with respect to the transition hazard attributable to the first-cohort membership, while keeping the q th covariate fixed at some value z_q across cohorts. The corresponding hazard ratio takes the form

$$\text{HR}_{g|z_q}^{\ell m} = \exp \left(\eta_g^{\ell m} + \eta_{g \times z_q}^{\ell m} z_q \right), \quad (9)$$

through which the test (8) can be once again performed.

3.3.2 | M2 Approach: Cohort stratification, allowing the cohort to interact with a covariate

For our M2 approach, we assume a stratum-cohort Cox model, with the cohort serving as the stratification variable. Each cohort's underlying risk is then characterized by its own baseline hazard function, while still sharing the estimated values for the

regression parameters. Consequently, the proportional hazards hypothesis may be said to hold within each cohort, but not across the cohorts. Under the M2 approach, the $\ell \rightarrow m$ transition hazard for a subject i belonging to the cohort $g = 1, \dots, G$ is given by

$$h_i^{\ell m}(t \mid \mathbf{z}_i, t_{\ell i}, c_{gi} = 1) = h_{0g}^{\ell m}(t) \exp \{ (\boldsymbol{\beta}^{\ell m})^\top \mathbf{z}_i + \gamma^{\ell m} t_{\ell i} + \eta_{g \times z_q}^{\ell m} z_{qi} \}, \quad (10)$$

where $h_{0g}^{\ell m}(t)$ is the baseline hazard function specific to the g th cohort. Note that the isolated cohort effect has now vanished, even though the model allows for estimating the way in which some covariate of interest z_q is modulated within a given cohort. Moreover, the hazard ratio associated with a Δ -unit increase in z_q is again conditioned on the cohort:

$$\text{HR}_{z_q \mid g}^{\ell m} = \exp(\eta_{g \times z_q}^{\ell m} \Delta). \quad (11)$$

Nonetheless, under M2 approach, comparison of transition hazards from subjects belonging to different cohorts with identical z_q cannot be done via a simple parameter. Rather, the expression for the hazard ratio becomes time-dependent in that case:

$$\text{HR}_{z_q \mid g}^{\ell m}(t) = \frac{h_{0g}^{\ell m}(t)}{h_{01}^{\ell m}(t)} \exp \{ (\eta_{g \times z_q}^{\ell m} - \eta_{1 \times z_q}^{\ell m}) z_q \}.$$

4 | ANALYSIS OF THE EMPIRICAL DATA FROM THREE COVID-19 WAVES

Based on Figure 1, the analysis of the div3W data is concerned with attaining a better characterization of the distinct COVID-19 waves. For covariate selection at a given transition, the main prognostic covariates to be possibly included are those of Table 1, along with the time of entry into the current state for non-Markovian transitions and the wave covariate within the M1 approach. Moreover, since interaction terms between wave and any covariate are allowed for M1 and M2 approaches, the quantitative prognostic covariates are centered around their means to preserve meaningful interpretations of their main effects. Thus, leaving aside the inclusion potential interactions, the main covariate effects to be considered are listed in Table 2.

Table 2 Potential baseline covariates to be included for modeling the $\ell \rightarrow m$ transition hazard from the div3W data, under M1 and M2 approaches.

Covariate notation	Meaning
sex (female)	Indicator for female
age (years)	Centered age
safi (units)	Centered safi value
t_ℓ (days)	Time of entry into the ℓ state
g (wave)	Wave factor, $g = 1, 2, 3$ (only for M1)

In a second phase, a minimum number of individuals per transition is checked in order to achieve reliable parameter estimates. In practice, this compels us to ensure a sufficiently large sample size for the number of parameters to be estimated. We have followed Vittinghoff & McCulloch (2007), who recommend that medical researchers consider at least five subjects per predictor within the Cox modeling setting. Using this general rule of thumb in our data, a given transition hazard will only consider the baseline hazard of occurrence whenever $n \leq 5$ in any of the three waves. If this threshold is surpassed in all waves, the transition hazard will accommodate as many prognostic covariates as possible from Table 2, starting with the inclusion of sex and age covariates as potential cofounders; they are often easy to measure, generally having few or no missing values.

The distinct transition hazards will be estimated under the M1 and M2 approaches, while examining the Markov property and the wave effect accommodation. Throughout, a significance level of 0.05 is adopted to examine the relevance of our results.

4.1 | Application of the global test for the key transitions

The Markov property, conditional on transition-specific covariates, is only assessed in certain transitions described by our empirical data. In that respect, note that transitions starting from the NSP state are inherently Markovian, and therefore excluded from any assessment. Moreover, in order to ensure worthwhile estimates, transitions involving $n \leq 5$ subjects in any wave are

not considered. Finally, the sojourn time in the recovery state has been previously set at 2 days, so the Markovian assessment is not carried out for trajectories starting or ending at this state. For the remaining transitions, a sequence of Cox-based log-rank tests is applied over a suitable grid of landmark times for both the M1 and M2 approaches. Adequately selecting the test grid, however, is often not a trivial task: highly unbalanced subsamples may arise at early times, while too-small subsample sizes can be obtained at the later ones. For each transition, p -values from different grids are compared to determine appropriate choices for the landmarks. This leads us to compute the test statistics over the follow-up interval $[t_0 = 1, t_{\max} = 10]$ for the SP \rightarrow NIMV and SP \rightarrow IMV transitions, while considering $[t_0 = 2, t_{\max} = 10]$ for the NIMV \rightarrow IMV and IMV \rightarrow death transitions. As information provided by covariates, the M1 and M2 approaches account for the same prognostic information within a given transition, while only differing in the way they deal with the wave effect. Further, three alternatives for summarizing the resulting vector of test statistics $\{\bar{U}^{\ell m(j)}(s, \beta^{\ell m}), s \in [t_0, t_{\max}]\}$ are considered: the mean, the weighted mean, and the supremum. In each case, the results are obtained from 2000 wild bootstrap resamples.

The p -value estimates of the global score test for all the transitions analyzed can be found in Sections A.1 – A.2 of Appendix A (Tables S1 – S2). For conciseness, Table 3 of the manuscript shows only the results derived from those transitions where the Markov property, conditional on observed covariates, is ultimately rejected in any of the COVID-19 waves: SP \rightarrow NIMV and SP \rightarrow IMV. Particularly, the overall p -values provide evidence to reject the Markov hypothesis for these transitions under the M1 and M2 approaches. Hence, the results for both approaches suggest that subject’s past history has a determining role when moving from SP to any one of the two states related to the need for mechanical ventilation, whereas these historical effects are not found to have an influence in the in the NIMV \rightarrow IMV and IMV \rightarrow death transitions for any of the waves. An intuitive explanation of this pattern is as follows. Considering that all the hospitalized subjects under study are, by definition, critically ill individuals with COVID-19, departures from the Markov assumption must be found in differences between baseline prognostic characteristics from subjects that were hospitalized without SP versus those with SP. That is, baseline covariates would become especially relevant in the first days following hospital admission. Nevertheless, as the multistate process moves forward and subjects reach more critical states, the possible past-history prognostic role vanishes progressively. In some sense, the health risk would tend to be similar for subjects occupying states far from hospital admission, so the NIMV \rightarrow IMV and IMV \rightarrow death transitions would become essentially Markovian conditional on observed baseline covariates.

Table 3 Results of the global score test for the assessment of the Markov property conditional on covariates, using both the M1 and M2 approaches to analyze the div3W data. The presentation of results is here restricted to the non-Markovian transitions, for which the global test provides p -value estimates both at each qualifying state and in overall terms, while considering three distinct summaries from families of log-rank statistics: unweighted mean (UM), weighted mean (WM), and the supremum (S).

Approach	Transition	Rule	Qualifying states				Overall
			NSP	SP	NIMV	IMV	
M1	SP \rightarrow NIMV	UM	<0.001	<0.001	–	–	<0.001
		WM	<0.001	<0.001	–	–	<0.001
		S	0.008	<0.001	–	–	<0.001
	SP \rightarrow IMV	UM	0.007	0.002	–	–	0.003
		WM	<0.001	<0.001	–	–	<0.001
		S	0.056	0.008	–	–	0.008
M2	SP \rightarrow NIMV	UM	<0.001	<0.001	–	–	<0.001
		WM	<0.001	<0.001	–	–	<0.001
		S	0.011	<0.001	–	–	<0.001
	SP \rightarrow IMV	UM	0.002	<0.001	–	–	<0.001
		WM	<0.001	<0.001	–	–	<0.001
		S	0.003	<0.001	–	–	<0.001

4.2 | Parameter estimates within the three-wave semi-Markov multistate model

Each of the transition hazards from the div3W data is modeled by separately fitting a Cox semiparametric model, under both the M1 and the M2 approaches. Whenever a given transition hazard involves a sufficiently large number of individuals in each of the three waves, all the mentioned covariates in Table 2 are included in the modeling procedure. Moreover, the significance of the different interactions between any of these covariates and the wave effect are sequentially checked via the corresponding bivariate test. For the sake of parsimony, in each transition hazard we only keep the interaction term with the smallest p -value, whenever p -value < 0.05 is obtained. Table 4 provides the distinct covariates considered when modeling each transition hazard, while indicating the p -value associated to the significant interaction term, if any, that is included. Furthermore, for those transitions in which the Markov assumption does not hold, i.e. $SP \rightarrow NIMV$ and $SP \rightarrow IMV$, the time to entry into SP, say t_{SP} , is included as an additional covariate. To assess the proper functional form $f(\cdot)$ through which t_{SP} should be incorporated, we can compare the performance of this covariate under two distinct shapes. Initially, one can assume the traditional linear assumption for this covariate on the log-hazard scale, i.e. $f(\cdot) = \text{Id}(\cdot)$. As an alternative, this linear assumption can be relaxed by embedding t_{SP} into a natural cubic spline basis. The two resulting fits can be then compared using a likelihood ratio test that informs us about possible nonlinear effects. This comparison is provided for both approaches in Section B.1 of Appendix B (Figures S1 – S2), allowing us to conclude that no particular transformation is needed for the inclusion of t_{SP} . The transition-specific point and 95% confidence interval (CI) estimates are provided in Section B.2 of Appendix B (Tables S3 – S4), and the corresponding hazard ratios (where each covariate is related to a prespecified Δ -unit increment) are found in Section B.3 (Tables S5 – S6). Furthermore, for a given transition-specific covariate, the proportional hazards assumption is graphically checked using a class of tests statistics based on cumulative sums of martingale-based residuals (Lin et al., 1993). Briefly, this conforms a multiparameter stochastic process that can be approximated by a zero-mean Gaussian process under the assumed model, so the observed pattern is compared with a number of simulated ones from the null distribution. Further, we can compute the Kolmogorov-type supremum statistic test based on a large number of realizations, reporting an estimate for the p -value of the test. The main advantage of this omnibus test, implemented in the R software by Martinussen & Scheike (2006), relies on the fact that no particular shape needs to be assumed when testing for lack of fit regarding a given covariate. For each transition and covariate, graphical plots of the score process over follow-up time are given in Section B.4 (Figures S3 – S22). In most transitions, the PH assumption is fulfilled, even though departures from proportionality are obtained for the safi and the cohort covariate under the M1 approach. Generally, these deviations are corrected for the most flexible approach M2.

Table 4 Baseline and historical characteristics to be accounted for when estimating each of the transition hazards from the div3W data under the M1 and M2 approaches.

Transition	Prognostic covariates	t_ℓ	Wave (M1)	Interaction (p -values)
(1) NSP \rightarrow SP	sex, age, safi	–	g	$g \times \text{safi}$ ($p_{M1} < 0.001, p_{M2} = 0.002$)
(2) NSP \rightarrow Discharge	sex, age, safi	–	g	–
(3) NSP \rightarrow Death	–	–	–	–
(4) SP \rightarrow Recovery	sex, age, safi	–	g	–
(5) SP \rightarrow NIMV	sex, age, safi	t_{SP}	g	$g \times \text{safi}$ ($p_{M1} = 0.002, p_{M2} = 0.001$)
(6) SP \rightarrow IMV	sex, age, safi	t_{SP}	g	$g \times \text{safi}$ ($p_{M1} = 0.041, p_{M2} = 0.088$)
(7) SP \rightarrow Death	–	–	–	–
(8) Recovery \rightarrow Discharge	sex, age, safi	–	g	–
(9) Recovery \rightarrow Death	–	–	–	–
(10) NIMV \rightarrow Recovery	sex, age, safi	–	g	–
(11) NIMV \rightarrow IMV	sex, age, safi	–	g	$g \times \text{age}$ ($p_{M1} = 0.016, p_{M2} = 0.009$)
(12) NIMV \rightarrow Death	–	–	–	–
(13) IMV \rightarrow Recovery	sex, age, safi	–	g	–
(14) IMV \rightarrow Death	sex, age, safi	–	g	–

Basically, within a given transition, the estimates derived from both approaches are found to be very similar. For the M1 and M2 approaches, the wave factor exhibits a significant interaction with the safi value within the earlier transitions. By contrast, in the later transitions, the presence of comorbidities at hospital entry do not report behavioral differences across waves: the

wave membership is shown to only interact significantly with the age covariate in the NIMV \rightarrow IMV transition. An explanation for this can be found in the fact that the first COVID-19 wave exhibits a younger subject profile in comparison with the second and third waves, wherein the need for supplemental oxygen is probably crucial to understanding a subject's transition from NIMV to IMV. Instead, upon entering into the IMV state, the subject's health status is severe enough that differences in age and comorbidity patterns between the waves do not seem to have a pivotal influence on the forward transitions.

For brevity, we next focus exclusively on the non-Markovian transition between $\ell = \text{SP}$ and $m = \text{NIMV}$ states to show how graphical tools can be used to analyze the numerical output obtained from a given transition. The time of entry into SP, t_{SP} , is incorporated as a historical covariate. Under the M1 approach, the SP \rightarrow NIMV transition hazard is modeled by specifying (6) as

$$\begin{aligned} h_i^{\ell m}(t \mid \text{sex}_i, \text{age}_i, \text{safi}_i, t_{\text{SP}i}, c_{gi} = 1) \\ = h_0^{\ell m}(t) \exp \left\{ \beta_{\text{sex}}^{\ell m} \text{sex}_i + \beta_{\text{age}}^{\ell m} \text{age}_i + \beta_{\text{safi}}^{\ell m} \text{safi}_i + \gamma^{\ell m} t_{\text{SP}i} + \eta_g^{\ell m} + \eta_{g \times \text{safi}}^{\ell m} \text{safi}_i \right\}, \end{aligned}$$

where the point estimates and 95% confidence intervals of the isolated wave effect are found to suggest an increasing propensity to receiving NIMV over the course of the pandemic: $\hat{\eta}_2^{\ell m} = 0.250$ ($-0.027, 0.527$) and $\hat{\eta}_3^{\ell m} = 0.311$ ($0.046, 0.586$). This apparently contradictory statement is actually consistent with the progressively less strict medical criteria for receiving advanced care: the relaxation of this criteria enabled access to NIMV for very ill subject profiles who would not have been admitted during the first wave.

By means of (7), the M1 approach provides the corresponding hazard ratio associated with a Δ -unit increase in the safi prognostic covariate:

$$\text{HR}_{\text{safi} \mid g}^{\ell m} = \begin{cases} \exp(\beta_{\text{safi}}^{\ell m} \Delta) & \text{for } g = 1, \\ \exp\left\{(\beta_{\text{safi}}^{\ell m} + \eta_{2 \times \text{safi}}^{\ell m}) \Delta\right\} & \text{for } g = 2, \\ \exp\left\{(\beta_{\text{safi}}^{\ell m} + \eta_{3 \times \text{safi}}^{\ell m}) \Delta\right\} & \text{for } g = 3. \end{cases}$$

For the M2 approach, the three waves form the natural groups for implementing our stratification. The SP \rightarrow NIMV transition hazard comes from particularizing (10) as

$$\begin{aligned} h_i^{\ell m}(t \mid \text{sex}_i, \text{age}_i, \text{safi}_i, t_{\text{SP}i}, c_{gi} = 1) \\ = h_{0g}^{\ell m}(t) \exp\left(\beta_{\text{sex}}^{\ell m} \text{sex}_i + \beta_{\text{age}}^{\ell m} \text{age}_i + \gamma^{\ell m} t_{\text{SP}i} + \eta_{g \times \text{safi}}^{\ell m} \text{safi}_i\right), \end{aligned}$$

where the wave effect itself vanishes from the analysis since it is used for stratification. The hazard ratio associated with an increase of Δ units in safi is concretized from (11) through

$$\text{HR}_{\text{safi} \mid g}^{\ell m} = \begin{cases} \exp(\eta_{1 \times \text{safi}}^{\ell m} \Delta) & \text{for } g = 1, \\ \exp(\eta_{2 \times \text{safi}}^{\ell m} \Delta) & \text{for } g = 2, \\ \exp(\eta_{3 \times \text{safi}}^{\ell m} \Delta) & \text{for } g = 3. \end{cases}$$

Figure 2 summarizes, as a forest plot, the hazard ratio estimates and 95% CI derived for the SP \rightarrow NIMV transition when fitting our data under M1 and M2. Interestingly, there is hardly any difference between the estimates obtained from both approaches. For the baseline prognostic covariates sex (female indicator) and age (taking increments of 5 years), the corresponding 95% CI contain the unit value, so we cannot conclude an effect in any case. On the other hand, the results from both approaches provide above-one hazard ratios associated to t_{SP} , with $\widehat{\text{HR}}_{\text{M1}} = 1.790$ and $\widehat{\text{HR}}_{\text{M2}} = 1.800$, respectively. However, for the sake of interpretation, we instead opt for displaying the results in terms of the sojourn time in SP, $t - t_{\text{SP}}$, yielding $\widehat{\text{HR}}_{\text{M1}} = 1/1.790 = 0.559$ and $\widehat{\text{HR}}_{\text{M2}} = 1/1.800 = 0.556$, with their corresponding 95% CI clearly below the hazard ratio threshold of one unit. There is consequently strong evidence for suggesting that the more time a subject passes in SP, the lower their risk for moving to NIMV. This makes sense, since very ill subjects tend to quickly require ventilatory support and so are more correlated with the risk of starting off with NIMV. It is worth noting that our approaches account for the interaction between the wave factor and the safi value (considering increments of $\Delta = 25$ units), thereby allowing us to interpret the association between the transition hazard and this covariate value, conditional on wave membership. Interestingly, the forest plot indicates not only that higher safi values are protective with respect to transitioning to NIMV, but also shows how the safi effect is modulated across the three COVID-19 waves. In particular, the expected protective impact of higher safi values increases progressively across the three waves: $1 > \text{HR}_{\text{safi} \mid 1}^{\ell m} > \text{HR}_{\text{safi} \mid 2}^{\ell m} > \text{HR}_{\text{safi} \mid 3}^{\ell m}$. That is, although a certain increase in safi reduces the hazard for moving from SP to

NIMV in all waves, a higher protective effect is observed among subjects in the second and third waves, which paradoxically comprise an increase in subject-specific comorbidities in comparison with the first wave. Rather, the reason for this difference in behavior between the waves resides in a better knowledge of the disease over time, yielding more reliable treatment results even when a subject enter the hospital with more deteriorated health conditions.

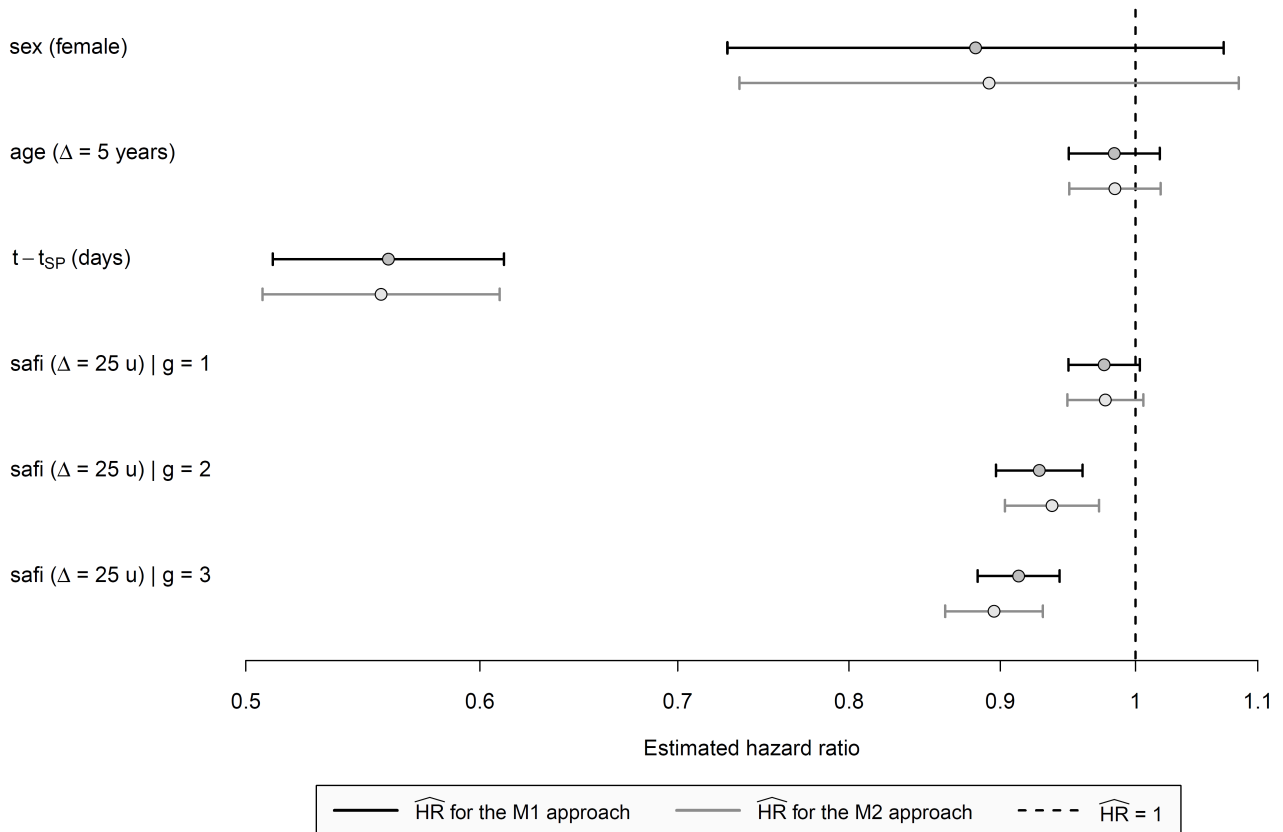


Figure 2 Hazard ratio estimates when the M1 and M2 approaches are employed to fit the hazard transition 5 (SP → NIMV) from the div3W data. Standard errors are obtained and used to construct the 95% confidence intervals.

As an interesting feature of the M1 approach, it allows for comparing the transition-specific hazard associated with belonging to either to the second or third wave versus being located in the first wave, conditional on a given covariate value. Coming back to the SP → NIMV transition, we can analyze how the transition hazard from SP to NIMV varies across waves according to the specific value attained by the safi baseline covariate. This leads (9) to being concretized as follows:

$$\text{HR}_{g|\text{safi}}^{\ell m} = \begin{cases} \exp(\eta_2^{\ell m} + \eta_{2 \times \text{safi}}^{\ell m} \text{safi}) & \text{for } g = 2, \\ \exp(\eta_3^{\ell m} + \eta_{3 \times \text{safi}}^{\ell m} \text{safi}) & \text{for } g = 3. \end{cases}$$

By using the above expression, Figure 3 illustrates how the estimated hazard ratios related to the second and third waves vary with respect to the first wave, conditioned on attaining a given safi value within the range [-100, 81.5]; this interval has been obtained from centering (around their mean) the original values observed for the safi prognostic covariate, the vast majority of which were placed within the range [300, 476.2]. Although both $\text{HR}_{2|\text{safi}}^{\ell m}$ and $\text{HR}_{3|\text{safi}}^{\ell m}$ lead to above-one quantities when a subject moves between $\ell = \text{SP}$ and $m = \text{NIMV}$ states, these two quantities depict similar decreasing patterns across the considered interval for safi. That is, their corresponding protective effect as regards going to NIMV becomes higher with the safi value. Further, conditional on a given safi, it should be noted that subjects who belong to the third wave have a higher hazard ratio in comparison to subjects who belong to the second wave. That is, the protective effect of moving to NIMV is smaller for a

third-wave subject. A possible explanation for this resides in the capability of treating subjects with more severe comorbidities during the third wave, who in counterpart would achieve a smaller protective effect at a given safi value due to having a more deteriorated health status at hospital entry. Hence, though the evolution of the disease knowledge cannot be directly observed, it does continuously play an underlying role when comparing results from different historical periods.

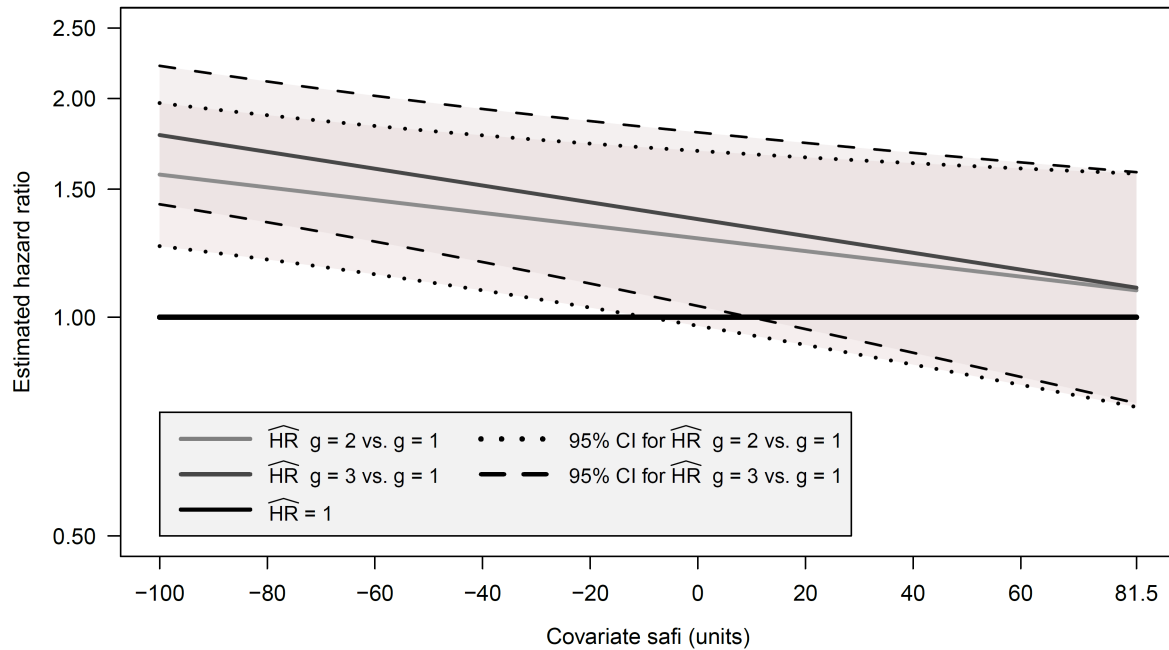


Figure 3 Within-wave evolution of the hazard ratio estimates when the M1 approach is employed to fit the hazard transition 5 (SP → NIMV) from div3W data, conditioned on the safi value. Standard errors are obtained and used to construct the 95% confidence intervals.

Likewise, Figure 4 illustrates the main strength of the M2 approach, allowing us to assess how each wave-specific baseline hazard evolves as a nuisance function upon entry into the SP state, from there moving into one of four potential states: discharge, NIMV, IMV, and death. This four-panel figure has a twofold illustrative purpose. Firstly, each of the four direct transitions under consideration conveys substantial information about the wave-related baseline hazard functions themselves. For instance, the panel devoted to the SP → discharge transition indicates that subjects from the first COVID-19 wave maintain a relatively constant underlying risk over the time interval $[0, 40]$ days, subsequently experiencing a sharp increase in the instantaneous risk of being discharged. This behavior differs substantially from the other two COVID-19 waves, which exhibit a gradual increase over time. A possible explanation for this discrepancy, as has been noted above, stems from the limitations in both the knowledge of the disease and the medical resources during the first wave, resulting in longer stays in the SP state for many of the hospitalized subjects. As a result, when fixing a reference point within the first 40 days of subjects' in-hospital stay, those belonging to the first wave have a lower underlying risk of being discharged than those in either the second or the third wave, when better COVID-19 treatments were readily available. Secondly, these plots as a whole provide a comprehensive picture of how the flows of subjects moving through different transitions are implicitly interrelated. Particularly, it is instructive to realize how the hazard of moving from SP to recovery increases within a 10-day period, with hardly any subjects moving to the NIMV, IMV, and death states after this period. In other words, we may infer that there is barely any risk of moving towards more critical states once a subject has remained in the SP state for approximately 10 days.

4.3 | Forecasting time-to-event outcomes for subject-specific profiles

Until now, the results have been largely discussed in terms of both covariate and cohort effects on a given transition hazard, based on either the M1 and M2 multistate modeling approaches. While these results are quite interesting by themselves, the multistate

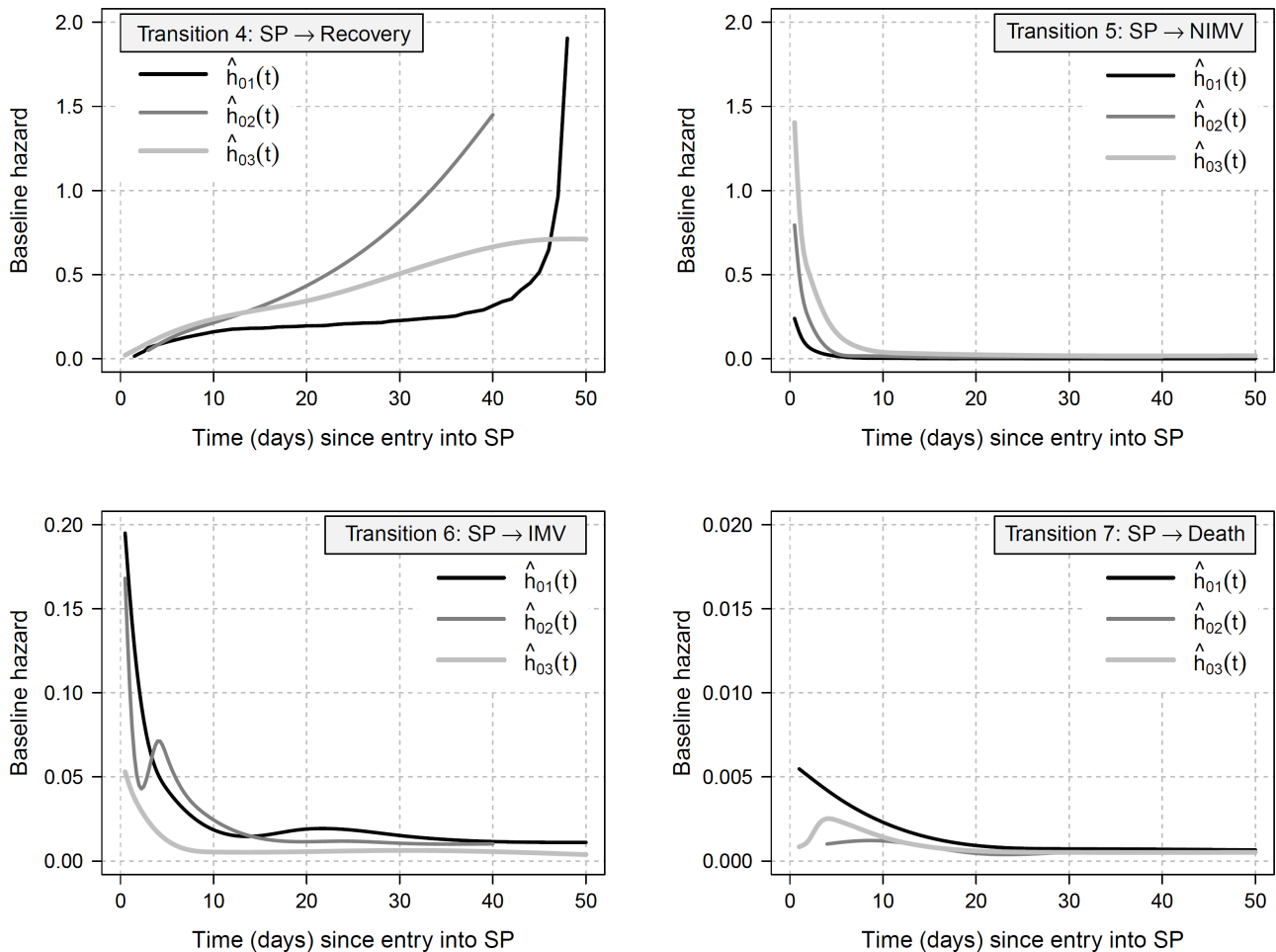


Figure 4 Smoothed estimates for the transition-specific baseline hazards per cohort using the M2 approach in the div3W data. Baseline hazards are particularly estimated for all subjects moving from the SP state towards subsequent states, regardless the time point t_{SP} at which a subject has entered into SP.

modeling framework also allows us to answer clinically important subject-specific questions involving multiple transitions, while conditioning on a set of personal characteristics. In particular, one of the most attractive features of the general multistate modeling framework relies on using the hazard transition estimates to compute individualized predictions for the event history process. These predictions for a subject's prognosis are indeed expected to be highly accurate since intermediate states in the whole process can be accounted for. Let us consider a fictitious subject, say k , from our target population but not included in our motivating dataset, known to occupy the ℓ state at time $s \geq 0$. We are interested in computing the subject-specific conditional probability of occupying a future state, say m , given a set of prognostic features at hospital entry, \mathbf{z}_k , the time of entry into the current state, $t_{\ell k}$, and the COVID-19 wave, $g = 1, 2, 3$:

$$P_k^{\ell m}(s, t) = \Pr\{X_k(t) = m \mid X_k(s) = \ell, \mathbf{z}_k, t_{\ell k}, c_{gk} = 1\}, \quad s < t.$$

When the Markov assumption does not hold in all transitions, empirical inferences regarding prediction probabilities can be still consistently derived from the non-parametric AJ estimator, given that censoring is not related to the states occupancy or to the transition times between states (Datta & Satten, 2001). Thus, the procedures implemented in the R package `mstate` remain valid for our purposes. Alternatively, using the same package, prediction probabilities can be performed by simulating a sufficiently large number of trajectories, say $M = 10000$, through the corresponding multistate setting.

For illustration, we retrospectively explore the evolution of two fictitious subject profiles from our target population. Particularly, let us consider two distinct medical profiles for a 50-year-old male, one low-risk and the other high-risk, whose health forecasting is expected to be vastly different. Regarding the safi covariate, the uncentered value for the low-risk profile is 476.2

units, whereas the high-risk profile has 410 units. Both subject trajectories are assumed to start from the SP state at time zero, while their quantitative covariates are accounted for after being centered around their corresponding means. We then focus on understanding how each profile’s medical information affects the probability of occupying any subsequent state during the hospitalization period. Of special relevance is the mortality forecasting of a subject, which in our multistate scheme is equivalent to estimating the probability of dying in the hospital.

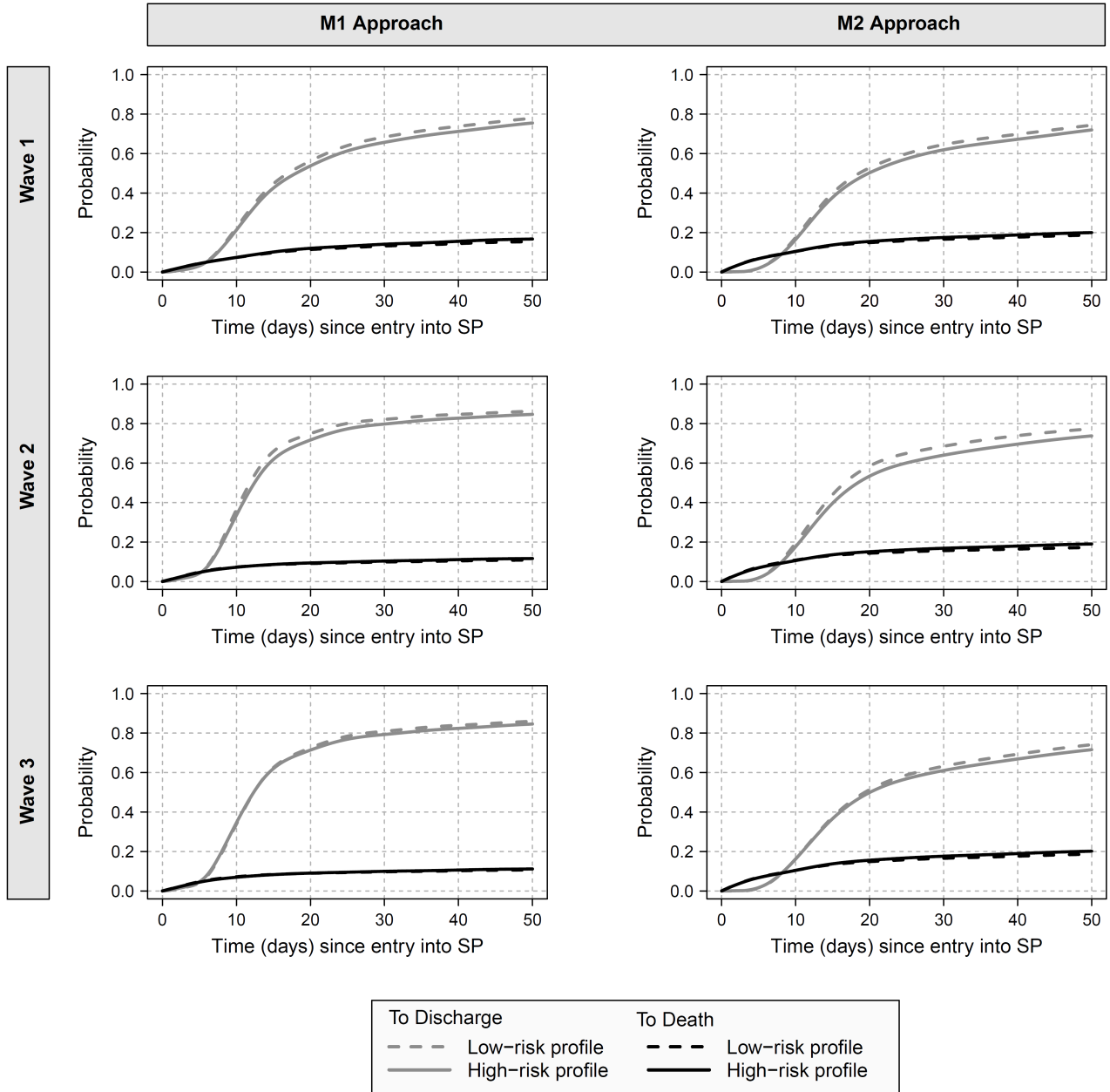


Figure 5 Smoothed estimates for the prediction probabilities related to the low-risk and high-risk profiles considered. Results are derived from both the M1 and M2 approaches and each of the three COVID-19 waves.

For the fictitious low-risk and high-risk profiles, Figure 5 shows the prediction probabilities computed from the M1 and M2 approaches within each of the three COVID-19 waves. In essence, the subject’s baseline features seem to have an influence when forecasting mortality risk, as evidenced in all the possible combinations of both the approach employed and the wave of

reference. For a given time t at which a prediction is to be made, a low-risk subject profile systematically gives rise to a higher probability of being discharged than the high-risk profile, and this relationship between profiles is just the opposite in regard to the probability of dying in the hospital. Equally important is quantifying the effect of the wave covariate when estimating prediction probabilities, in which the first wave yields smaller differences between survivors and nonsurvivors within the M1 approach. A plausible explanation for this pattern must be found in the limited knowledge of the disease in the first wave, giving rise to a higher number of in-hospital deaths in comparison with second- and third-wave pandemic periods. Also note that, for any of the waves under M2, differences between survivors and nonsurvivors clearly diminish with respect to M1. Therefore, it is clear the influence of the wave covariate itself to predict state occupation probabilities.

To quantify the departure between the probability of being discharged and dying, the prediction probabilities for low- and high-risk profiles can be evaluated at distinct time points after experiencing SP. In our data, subjects entering the hospital at SP show a median overall stay of 15 days (mean of 22.5 days), so $t = 10$ and $t = 20$ days are reasonable choices. Prediction results can be consulted in Table S7 of Appendix C.

To conclude this section, another point worth mentioning is the dynamic behavior of the prediction probabilities. In practice, this means that future trends for a particular subject profile can be updated as new information becomes available during the hospitalization period. To exemplify this dynamic forecasting using the two risk profiles considered, Figures S23–S24 of Appendix C shows the evolution of the prediction probabilities as a given subject profile enters later in the SP state. Hence, given a particular low-risk and high-risk subject profile who entered into the SP state at $t \in \{0, 5, 10\}$ days, the probabilities of either being discharged or dying are computed for the M1 and M2 approaches.

5 | DISCUSSION

A covariate-cohort approach, M1, and a stratum-cohort approach, M2, have been proposed as Cox-based multistate modeling strategies to analyze event history data from different cohorts. These approaches postulate alternative ways to properly accommodate the heterogeneity across distinct subpopulations, since subjects belonging to the same cohort tend to share unobserved characteristics that cannot be explicitly accounted for. The M1 covariate-cohort approach considers a collection of cohort-specific binary indicators, serving as proxies for collecting within-cohort unobserved characteristics. As an alternative strategy, the M2 stratum-cohort approach delves deeper into explaining within-cohort subject behavior by means of allowing an extra flexibility to estimate transition-specific underlying risks for different cohorts. While M1 is more often preferred when the cohort-specific covariate effects are of main interest, M2 is more likely to be chosen when the research focus is on transition probabilities. A further advantageous aspect to mention in M2 approach is that stratifying the event history data by group eases compliance with the proportional hazards hypothesis. Nonetheless, the cohort effect can be neither estimated nor statistically tested, since it is used for stratification. On another note, the Markov property conditional on covariates has been assessed using a global score test. Whenever a non-Markov environment is detected, the time of entry into the current state are included in the corresponding Cox model, setting our analysis into a semi-Markov framework. The relevance of this time-to-entry covariate is easily evaluated by performing a likelihood ratio test to assess whether the corresponding regression parameter is different from zero. Based on this rationale, the two testing procedures applied should be understood as complementary: the global score test serves as a pre-test for the Markovian condition, while the incorporation of the time-of-entry covariate offers a simple alternative for effectively considering a specific aspect of previous history.

The two suggested approaches have been applied to analyze a large sample of COVID-19-hospitalized subjects grouped into three distinct pandemic waves, all occurring in the southern Barcelona metropolitan area during the prevaccine era. The assessment of the Markov property in our multistate process revealed non-Markovianity for the transitions from severe pneumonia to noninvasive mechanical ventilation and invasive mechanical ventilation. As a consequence, the time of entry into the SP state, t_{SP} , has been incorporated as an explanatory covariate when modeling the transition hazard. The relationship between t_{SP} and the transition hazard led us to conclude that later entry times into the SP state or, equivalently, shorter sojourn times, are strongly associated with a higher risk of requiring mechanical ventilation, either NIMV or IMV. In parallel, the presumed dependence among subjects in the same wave has been inspected using the two previously mentioned strategies for accommodating wave influences. Concerning the impact of the covariates on a given transition, parameter estimates under the M1 fixed-effects approach appear to parallel those derived under the M2 wave-stratified approach, and the same can be said for the corresponding standard errors. In fact, in the near absence of non-proportional wave-specific baseline hazards, these practically equivalent estimates could be anticipated since both approaches assume a multiplicative relationship between the covariates and the hazard function.

The analysis of our empirical COVID-19 data involves distinct critical considerations that must be pointed out. First, our three waves were not randomly sampled, but were rather gathered during a very specific historical disease period, within a particular geographic area. Hence, for more general conclusions to be drawn, it would be interesting to consider data in other geographical areas during the same disease period. Second, the different disease patterns observed across waves are largely due to the particular hospital protocol adopted within a given pandemic period (Straw et al., 2021). More specific guidance would therefore be necessary in this respect to better understand the ceiling of care criterion employed in each period. For instance, one additional source of information could be hospital-bed occupancy rates (Bekker et al., 2023). Additionally, the treatments employed have also changed over the course of the pandemic; a paradigmatic example is the use of corticosteroids, whose extended administration to hospitalized subjects since the second wave led to a large improvement in the effectiveness of COVID-19 treatment (Balaz et al., 2021). In our case, a careful comparison between the characteristics of wave-specific subjects has enabled us to explain, whether through the M1 or M2 approach, the later differences observed in the behavior of each wave. A further key point of our dataset is the time that a subject recovers from COVID-19, which is actually unobserved. Instead, it has been assumed that recovery occurs two days prior to discharge. An alternative would consist of considering a latent recovery state, which would be omitted when fitting the Cox-based multistate models. In practice, this would entail the disappearance of the recovery \rightarrow discharge and recovery \rightarrow death transitions, leaving the same number of subjects moving in transitions that did not involve the recovery state. Among the transitions with the required sample size for obtaining parameter estimates, only in the NSP \rightarrow SP and NSP \rightarrow discharge transitions the results would remain unchanged.

In addition to explaining subject-specific disease trajectories, we have obtained individualized prediction probabilities from the model fitted under both approaches. The presence of semi-Markov effects obviously makes this more difficult, although the non-parametric AJ estimator still guarantees consistent estimates. Thus, although the two approaches cannot be directly compared, it is possible to graphically compare the estimates for the state occupation probabilities. As an interesting alternative, Crowther and Lambert (2017) use a simulation-based method in the context of parametric models, wherein a wide variety of candidate models is available. A detailed comparison of the inference performance of both procedures could be a valuable line of future research to reach a better understanding of subject trajectories over the entire multistate process.

In conclusion, the identified trade-offs between the M1 and M2 approaches do not necessarily imply raising the question of whether one of the approaches is preferable to the other. On the contrary, we could argue that this is not a dichotomous choice at all, since both semi-Markovian approaches represent reliable and easy-to-implement alternatives to analyze multicohort data in the multistate framework. More generally, given a certain dataset to be analyzed, the selection of one or the other approach will depend on both which cohort-specific key aspects are to be highlighted and the focus of the inference.

ACKNOWLEDGMENTS

This research was partially supported by grants from the Spanish Ministry of Science and Innovation (PID2019-104830RB-I00) and from the Catalan Department of Research and Universities (2020PANDE00148). The authors are very grateful to Professor A. C. Titman for his outstanding help in clarifying some aspects of the Cox-based global test for checking the Markov hypothesis. The members of the Divine project to identify COVID-19 risk factors are the following (alphabetically ordered by last name): G. Abelenda-Alonso, M. Besalú, J. Carratalà, E. Cobo, J. Cortés, D. Fernández, L. Garmendia, G. Gómez Melis, C. Gudiol, P. Hereu, K. Langohr, G. Molist, N. Pallarès, N. Pérez-Álvarez, X. Piulachs, A. Rombaut, C. Tebé, and S. Videla.

CONFLICT OF INTEREST

The authors declare no potential conflicts of interest.

SUPPORTING INFORMATION

The web-based supplementary information contains the tables and figures reported by the aforementioned appendices A, B, and C. Moreover, the R code implementing our two modeling approaches are provided in Appendix D. Particularly, Section D.1 provides the code to perform the global testing procedure for the Markov property, Section D.2 the code for parameter estimates, Section D.2 the code for hazard ratio estimates, and Section D.4 shows how to compute predictions.

References

1. Andersen, A., & Keiding, N. (2002). Multi-state models for event history analysis. *Statistical Methods in Medical Research*, *11*(2), 91–115.
2. van Houwelingen, W.C., & Putter, H. (2008). Dynamic predicting by landmarking as an alternative for multi-state modeling: An application to acute lymphoid leukemia data. *Lifetime Data Analysis*, *14*(4), 447–463.
3. Meira-Machado, L., de Uña-Álvarez, J., Cadarso-Suárez, C., & Andersen, P.K. (2009). Multistate models for the analysis of time-to-event data. *Statistical Methods in Medical Research*, *18*(2), 195–222.
4. Geskus, R.B. (2015). *Data Analysis with Competing Risks and Intermediate States*. Chapman & Hall/CRC: Boca Raton, Florida (USA).
5. Cook, R.J. & Lawless, J.F. (2018). *Multistate Models for the Analysis of Life History Data*. Chapman & Hall/CRC: Boca Raton, Florida (USA).
6. Darroch, J.N. & McCloud, P.I. (1990). Separating two sources of dependence in repeated influenza outbreaks. *Biometrika*, *77*(2), 237–243.
7. Birkenbihl, R.J., Salimi, S., Frohlich, H., Japanese Alzheimer’s Disease Neuroimaging Initiative, & Alzheimer’s Disease Neuroimaging Initiative. (2022). Unraveling the heterogeneity in Alzheimer’s disease progression across multiple cohorts and the implications for data-driven disease modeling. *Alzheimer’s & Dementia*, *18*(2), 251–261.
8. Freijser, L., Annear, P., Tenneti, N., Gilbert, K., Chukwujekwu, O., Hazarika, I., & Mahal, A. (2023). The role of hospitals in strengthening primary health care in the Western Pacific. *The Lancet Regional Health - Western Pacific*, *33*, 1–8.
9. Gelman, A., & Hill, J. (2007). *Data Analysis Using Regression and Multilevel/Hierarchical Models*. Cambridge University Press, Cambridge (UK).
10. Huang, C, Wang, Y, Li, X, Ren, L., Zhao, J., Hu, Y., ...Cao, B. (2020). Clinical features of patients infected with 2019 novel coronavirus in Wuhan,China. *The Lancet*, *395*(10223), 497–506.
11. Chan, J.F., Yuan, S., Kok K.-H., Kai-Wang To, K., Chu, H., Yang, J., . . . , Yuen, K.-Y. (2020). A familial cluster of pneumonia associated with the 2019 novel coronavirus indicating person-to-person transmission: a study of a family cluster. *The Lancet*, *395*(10223), 514–523.
12. Carbonell, R., Urgeles, S., Rodríguez, A., Bodí, M., Martín-Loeches, I., Solé-Violán, J., . . . , COVID-19 SEMICYUC Working Group. (2021). Mortality comparison between the first and second/third waves among 3,795 critical COVID-19 patients with pneumonia admitted to the ICU: A multicentre retrospective cohort study. *The Lancet Regional Health - Europe*, *11*(100243), 1–9.
13. Buttenschon, H.N., Lynggaard, V., Sandbøl, S.G., Glassou, E.N., & Haagerup, A. (2022). Comparison of the clinical presentation across two waves of COVID-19: A retrospective cohort study. *BMC Infectious Diseases*, *22*(423), 1–11.
14. Pallarès, N., Tebé, C., Abelenda-Alonso, G., Rombauts, R., Oriol, I., Simonetti, A.F., . . . , MetroSud and Divine study groups. (2023). Characteristics and outcomes by ceiling of care of subjects hospitalized with COVID-19 during four waves of the pandemic in a metropolitan area: a multi-center cohort study. *Infectious Diseases and Therapy*, *12*(1), 273–289.
15. Wendel-Garcia, P.D., Aguirre-Bermeo, H., Buehler, P.K., Alfaro-Farias, M., Yuen, B., David, S., . . . , Ristic, A. (2021). Implications of early respiratory support strategies on disease progression in critical COVID-19: a matched subanalysis of the prospective RISC-19-ICU cohort. *Critical Care*, *25*(1), 1–12.
16. Berenguer, J., Borobia, A.M., Ryan, P., Rodríguez-Baño, J., Bellón, JM, Jarrín, I., . . . , COVID@HULP Working Group. (2021). Development and validation of a prediction model for 30-day mortality in hospitalised patients with COVID-19: the COVID-19 SEIMC score. *Thorax*, *76*(9), 920–929.

17. Catoire, P., Tellier, E., de la Rivière, C., Beauvieux, M.C., Valdenaire, G., Galinski, M., Revel, P., Combes, X., & Gil-Jardiné, C. (2021). Assessment of the SpO₂/FiO₂ ratio as a tool for hypoxemia screening in the emergency department. *The American Journal of Emergency Medicine*, 44(23), 116–120.
18. Aalen, O.O., & Johansen, S. (1978). An Empirical Transition Matrix for Non-Homogeneous Markov Chains Based on Censored Observations. *Scandinavian Journal of Statistics*, 5(3), 141–150.
19. Cox, D.R. (1972). Regression models and life tables (with Discussion). *Journal of the Royal Statistical Society: Series B*, 34(2), 187–220.
20. Andersen, P.K., Hansen, L.S., & Keiding, N. (1991). Non- and semi-parametric estimation of transition probabilities from censored observation of a non-homogeneous Markov process. *Scandinavian Journal of Statistics*, 18(2), 153–167.
21. Meira-Machado, L., de Uña-Álvarez, J., & Cadarso-Suárez, C. (2006). Nonparametric estimation of transition probabilities in a non-Markov illness-death model. *Lifetime Data Analysis*, 12(3), 325–344.
22. Andersen, A., & Perme, M.P. (2008). Inference for outcome probabilities in multi-state models. *Lifetime Data Analysis*, 14(4), 405–431.
23. Titman, A. (2015). Transition Probability Estimates for Non-Markov Multi-State Models. *Biometrics*, 71(4), 1034–1041.
24. Breslow, N.E. (1972). Contribution to the Discussion of the paper by D. R. Cox. *Journal of the Royal Statistical Society: Series B*, 34(2), 216–217.
25. Putter, H., Fiocco, M., & Geskus, R.B. (2007). Tutorial in biostatistics: Competing risks and multi-state models. *Statistics in Medicine*, 26(11), 2389–2430.
26. Ieva, F., Jackson, C.H., & Sharples, L.D. (2017). Multi-state modelling of repeated hospitalisation and death in patients with heart failure: The use of large administrative databases in clinical epidemiology. *Statistical Methods in Medical Research*, 26(3), 1350–1372.
27. de Wreede, L.C., Fiocco, M., & Putter, H. (2010). The mstate Package for Estimation and Prediction in Non- and Semi-Parametric Multi-State and Competing Risks Models. *Computer Methods and Programs in Biomedicine*, 99(3), 261–274.
28. de Uña-Álvarez, J., & Meira-Machado, L. (2015). Nonparametric Estimation of Transition Probabilities in the Non-Markov Illness-Death Model: A Comparative Study. *Biometrics*, 71(2), 364–375.
29. Putter, H., & Spitoni, C. (2018). Non-parametric estimation of transition probabilities in non-Markov multi-state models: The landmark Aalen–Johansen estimator. *Statistical Methods in Medical Research*, 27(7), 2081–2092.
30. Titman, A.C., & Putter, H. (2022). General tests of the Markov property in multi-state models. *Biostatistics*, 23(2), 380–396.
31. Mammen, E. (1993). Bootstrap and Wild Bootstrap for High Dimensional Linear Models. *Annals of Statistics*, 21(1), 255–285.
32. Vittinghoff, E., & McCulloch, C.E. (2007). Relaxing the Rule of Ten Events per Variable in Logistic and Cox Regression. *American Journal of Epidemiology*, 165(6), 710–718.
33. Lin, D.Y., Wei, L.J., & Ying, Z. (1993). Checking the Cox model with cumulative sums of martingale-based residuals. *Biometrika*, 80(3), 557–572.
34. Martinussen, T., & Scheike, T.H. (2006). *Dynamic Regression Models for Survival Data*. *Statistics for Biology and Health*. Springer, New York (USA).
35. Datta, S., & Satten, G.A. (2001). Validity of the Aalen–Johansen estimators of stage occupation probabilities and Nelson–Aalen estimators of integrated transition hazards for non-Markov models. *Statistics & Probability Letters*, 55(4), 403–411.

36. Straw, S., McGinlay, M., Drozd, M., Slater, T.A., Cowley, A., Kamalathan, S., . . . , Witte, K.K. (2021). Advanced care planning during the COVID-19 pandemic: ceiling of care decisions and their implications for observational data. *BMC Palliative Care*, 20(10), 1–11.
37. Bekker R., uit het Broek, M., & Koole, G. (2023). Modeling COVID-19 hospital admissions and occupancy in the Netherlands. *European Journal of Operational Research*, 304(1) , 207–218.
38. Balaz, D, Wikman-Jorgensen, PE, Giner, V, Rubio-Rivas, M., de Miguel, B., Noureddine, M., . . . , Casas-Rojo, J.M. (2021). Evolution of the Use of Corticosteroids for the Treatment of Hospitalised COVID-19 Patients in Spain between March and November 2020: SEMI-COVID National Registry. *Journal of Clinical Medicine*, 10(19) , 1–17.
39. Crowther, M.J., & Lambert, P.C. (2017). Parametric multistate survival models: Flexible modelling allowing transition-specific distributions with application to estimating clinically useful measures of effect differences. *Statistics in Medicine*, 36(29) , 4719–4742.

